# The metastasis gene NEDD9 product acts through integrin β3 and Src to promote mesenchymal motility and inhibit amoeboid motility

**Jessica Ahn, Victoria Sanz-Moreno* and Christopher J. Marshall‡**

Division of Cancer Biology, Institute of Cancer Research, Cancer Research UK Centre Tumour Cell Signalling Unit, 237 Fulham Road, London SW3 6JB, UK

*Present address: Randall Division of Cell and Molecular Biophysics, New Hunt's House, Guy's Campus, London SE1 1UL, UK
‡Author for correspondence (Chris.Marshall@icr.ac.uk)

*Accepted 22 November 2011*
*Journal of Cell Science 125, 1814–1826*

*doi: 10.1242/jcs.101444*

## Summary

Neural precursor expressed, developmentally down-regulated 9 (NEDD9), a member of the Cas family of signal transduction molecules, is amplified at the genetic level in melanoma, and elevated expression levels have been shown to correlate with melanoma progression and metastasis. NEDD9 interacts with the guanine nucleotide exchange factor DOCK3 to promote Rac activation and the elongated, mesenchymal-type of tumour cell invasion, but the molecular mechanisms through which NEDD9 promotes melanoma metastasis are not fully understood. We show that signalling through increased NEDD9 levels requires integrin β3 signalling, which leads to elevated phosphorylation of integrin β3. This results in increased Src and FAK but decreased ROCK signalling to drive elongated, mesenchymal-type invasion in environments that contain vitronectin. NEDD9 overexpression does not affect ROCK signalling through activation of RhoA but decreases ROCKII signalling through Src-dependent phosphorylation of a negative regulatory site Tyr722. In NEDD9-overexpressing melanoma cells, inhibition of Src with dasatinib results in a switch from Rac-driven elongated, mesenchymal-type invasion to ROCK-dependent rounded, amoeboid invasion. These findings brings into question whether dasatinib would work as a therapeutic agent to block melanoma invasion and metastasis. On the basis of the in vitro data presented here, a combination treatment of dasatinib and a ROCK inhibitor might be a better alternative in order to inhibit both elongated, mesenchymal-type and rounded, amoeboid motility.

**Key words:** NEDD9, Src, Metastasis, Melanoma, Integrin

## Introduction

Neural precursor expressed, developmentally down-regulated 9 (NEDD9; also known as HEF-1 or Cas-L) is a member of the Crk-associated substrate (Cas) family of signal transduction proteins (Astier et al., 1997; Manie et al., 1997). The Cas family members have an N-terminal SH3 domain, a substrate domain containing multiple tyrosine phosphorylation site motifs, a serine-rich domain and a C-terminal helix-loop-helix motif. Integrin β1 signalling has been shown to lead to tyrosine phosphorylation of the substrate domain of NEDD9 in T cells (Minegishi et al., 1996) and B cells (Manie et al., 1997). In the substrate domain of NEDD9 are putative binding sites for the SH2 domains of adapter proteins such as CrkI, CrkII, CrkL, Nck and Abl (Sakai et al., 1994; Ishino et al., 1995; Nojima et al., 1995; Harte et al., 1996; Law et al., 1996; Minegishi et al., 1996; Petruzzelli et al., 1996; Salgia, 1996; Manie et al., 1997). In addition to potential roles in integrin signalling, NEDD9 has also been implicated in TNFα-induced apoptosis (Law et al., 2000) and cell cycle control where its association with Aurora A leads to the phosphorylation and activation of Aurora A (Pugacheva and Golemis, 2005).

Many studies implicate NEDD9 in cancer. NEDD9 expression has been found to be elevated in adult T-cell leukaemia (Iwata et al., 2005) and ovarian cancer (Donninger et al., 2004); NEDD9 has been shown to play a supportive role in tumour initiation in the MMTV-polyoma virus middle T mammary tumour model (Izumchenko et al., 2009). Overexpression of NEDD9 has been linked to tumour progression. Gene amplification is associated with increased metastasis in a mouse model of melanoma, and increased expression has been correlated with metastasis in human melanoma (Kim et al., 2006). Analysis of gene expression in primary lung carcinomas showed *NEDD9* is part of a metastasis signature (Minn et al., 2005). In colorectal cancer, *NEDD9* is a TCF–β-catenin target gene and elevated expression correlates with increased migration and cancer progression (Li et al., 2011). Additionally in colorectal cancer, *NEDD9* has been found to be a HIF-1α-regulated gene that mediates hypoxia-induced tumour cell migration (Kim et al., 2010). NEDD9 activity has also been shown to be required for invasive behaviour of glioblastomas (Natarajan, 2006).

These studies implicate overexpression of *NEDD9* in mechanisms of tumour spread. Previously we have shown that NEDD9 complexes with a guanine nucleotide exchange factor, DOCK3, to activate the Rho family GTPase, Rac1, in migration of melanoma cells (Sanz-Moreno et al., 2008). NEDD9–DOCK3–Rac signalling drives an elongated, mesenchymal-type of cell movement that is dependent on actin assembly and involves proteolysis to degrade the extra-cellular matrix (Friedl

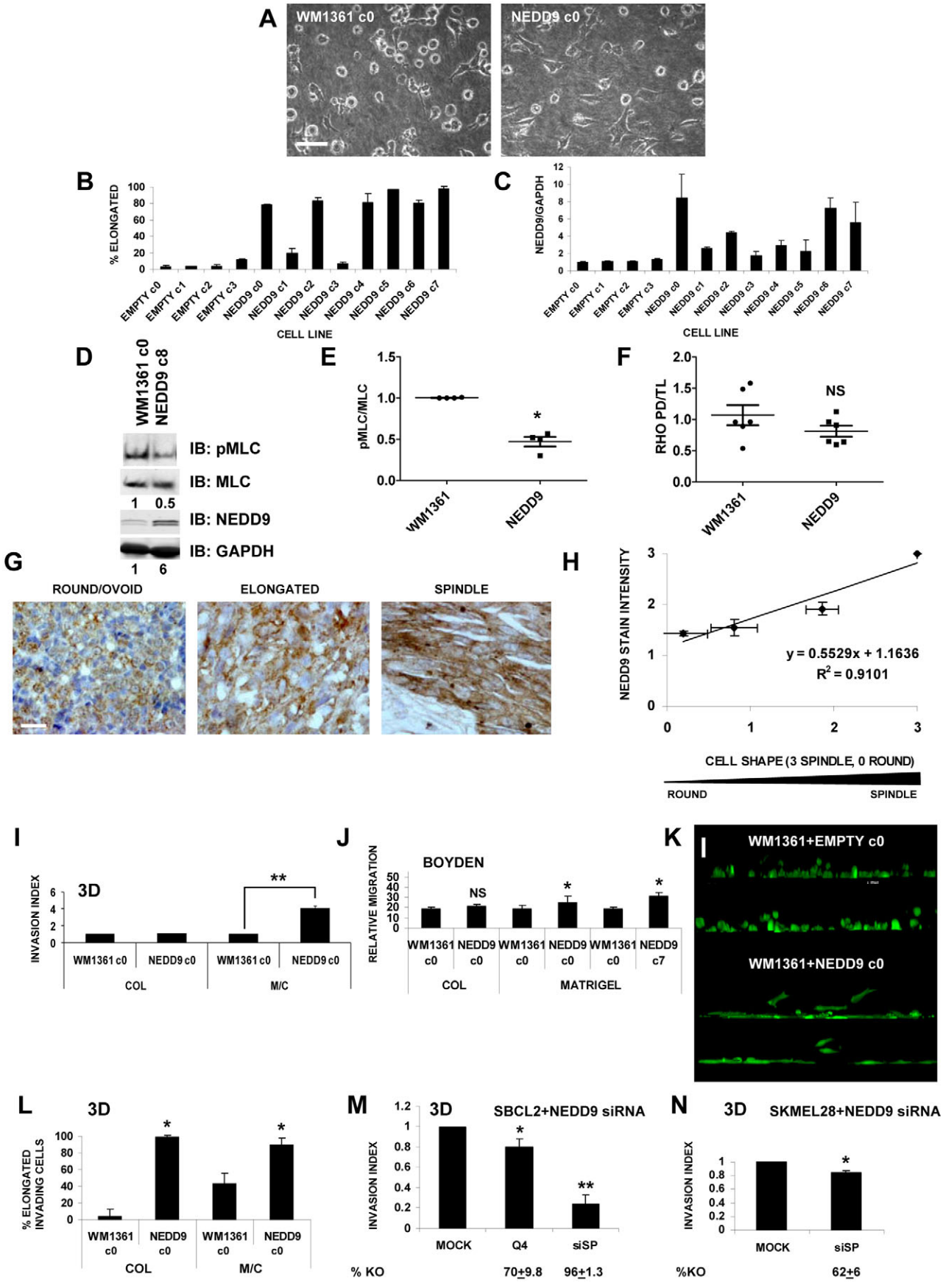


**Fig. 1.** See next page for legend.

and Wolf, 2010). In an alternative form of tumour cell movement referred to as rounded, amoeboid, cells squeeze through pre-existing gaps in the matrix by using actomyosin contractility generated by high Rho–ROCK signalling (Sahai and Marshall, 2003; Wolf et al., 2003; Sanz-Moreno et al., 2008; Friedl and Wolf, 2010). High actomyosin contractility and NEDD9-dependent Rac activation act as switches between elongated and rounded forms of movement. Rac activation opposes the high actomyosin contractility required for rounded, amoeboid movement whereas actomyosin contractility activates a Rac GTPase-activating protein, ARHGAP22, to inactivate Rac (Sanz-Moreno et al., 2008).

Although NEDD9 has been shown to participate in Rac-dependent elongated cell movement, much of the mechanism remains unclear. In this study we have investigated mechanisms of NEDD9-driven signalling.

## Results

### NEDD9 overexpression drives elongated morphology and elongated, mesenchymal-type invasion

To provide an assay for the effects of increased NEDD9 expression, which occurs in a number of cancers, we investigated the effects of overexpression on cell morphology. WM1361 melanoma cells have a predominantly round morphology driven by high actomyosin contractility when plated on a deformable matrix composed of growth-factor-reduced Matrigel and collagen-I (M/C); following transfection with a NEDD9 expression plasmid the proportion of elongated cells was increased (Fig. 1A–C). NEDD9 overexpression promoted Rac1 activation to the GTP-bound form (supplementary material Fig. S1A). As expected from previous work (Sanz-Moreno et al., 2008) NEDD9-driven cell elongation requires DOCK3 and Rac1 (supplementary material Fig. S1B,C). Elongated, mesenchymal-type movement is associated with lower levels of actomyosin contractility than rounded, amoeboid motility (Sanz-Moreno et al., 2008); accordingly myosin light chain-2 (MLC) phosphorylation was decreased with NEDD9 overexpression (Fig. 1D,E). Interestingly this reduction in MLC phosphorylation occurred with no apparent change in RhoA-GTP levels (Fig. 1F). This contrasts with a number of studies that show an inverse relationship between Rac1 and RhoA activation (Sander et al., 1999). To determine whether in a human melanoma cell line that uses elongated, mesenchymal-type movement NEDD9 depresses actomyosin contractility we silenced *NEDD9* expression by RNA interference in SKMEL2 cells. Silencing *NEDD9* led to elevated phosphorylation of MLC (supplementary material Fig. S1D,E).

To extend these observations on the effects of NEDD9 overexpression we examined human patient samples. From histopathology studies melanomas are known to consist of elongated, spindle or round, epithelioid cells (Rosai and Ackerman, 2004). Interestingly, examination of a tissue microarray containing 55 malignant melanomas, 19 metastatic melanomas and 23 primary melanomas for NEDD9 expression showed a strong correlation between NEDD9 levels and elongated morphology (Fig. 1G,H). Statistically significant correlation was seen between increases in staining intensity for NEDD9 and the different cell shapes, from round to ovoid, elongated and spindle. Thus in human melanomas NEDD9 overexpression is associated with a more elongated cell morphology.

We assayed WM1361 control and NEDD9-overexpressing cell lines for invasion and cell migration. Consistently, we found that NEDD9-overexpressing cell lines invaded significantly more ($P<0.01$) than WM1361 controls into three-dimensional (3D) matrices composed of Matrigel and collagen-1 (M/C) and showed increased migration in Boyden chamber assays with Matrigel compared with collagen-I (Fig. 1I,J). Confocal microscopy of cells invading a 3D matrix revealed that NEDD9-overexpressing cells were elongated rather than rounded (Fig. 1K,L). Knockdown of NEDD9 in the overexpression lines reversed the increase in invasion into Matrigel-containing matrices (supplementary material Fig. S1F). To extend these results on cell migration and invasion to human melanoma cell lines that move using elongated, mesenchymal-type motility, we used RNA interference to knockdown NEDD9 in the cell lines SBCL2 and SKMEL28. Knockdown of NEDD9 decreased invasion into M/C (Fig. 1M,N).

These results show that elevated expression of NEDD9 converts melanoma cells with a rounded morphology associated with high actomyosin contractility to an elongated morphology. Interestingly, enhanced invasion in 3D or cell migration in Boyden chambers following overexpression of NEDD9 was not observed when the matrix consisted solely of collagen-I (Fig. 1I,J). This suggests that NEDD9 signalling to promote invasion and cell migration requires a specific component of Matrigel and that NEDD9 signalling depends on the composition of the extra-cellular matrix.

**Fig. 1. NEDD9 overexpression drives elongated morphology and elongated, mesenchymal-type invasion.** (**A**) Images of WM1361 GFP control cell line 0 and NEDD9-overexpressing cell line 0 at 16 hours post plating on thick deformable matrix composed of collagen-I and Matrigel (referred to as M/C). Scale bar: 100 µm. (**B**) Percentage of elongated WM1361 GFP control and NEDD9-overexpressing cells on M/C, 16 hours post plating. 200 cells were scored per experiment; values are means ± s.e.m., $n=3$. (**C**) Quantification of immunoblot of NEDD9 expression level in WM1361 GFP control and NEDD9-overexpressing cell lines collected from M/C; values are means ± s.e.m. (**D**) Immunoblot of phosphorylated MLC and NEDD9 from the WM1361 GFP control cell line 0 and NEDD9-overexpressing cell line 8, 2 hours post plating on serum-free M/C. (**E**) Quantification of phosphorylated MLC normalised against total MLC in control and NEDD9-overexpressing lines, shown as a scatter plot. (**F**) Scatter plot of GTP-bound RhoA in control and NEDD9-overexpressing lines 2 hours post plating on collagen-I with 5% serum. (**G**) NEDD9-stained melanoma tissue microarray cores with ovoid to round cells, elongated cells and spindle-shaped cells. Scale bar: 10 µm. (**H**) Correlation between NEDD9 staining intensity and cell shape in a melanoma tissue microarray. Entire cores (1 mm diameter) were examined and given values of 0–3 for stain intensity and cell shape. For cell shape, cores were scored as 3 for spindle, 2 for elongated, 1 for ovoid and 0 for round. Stain intensity was scored as 3 for highest intensity and 0 for lowest intensity. NEDD9 intensity for a given shape score was averaged and all data analysed using linear regression. The correlation coefficient ($R^2$ value) is greater than 0.9. (**I**) 3D invasion by control WM1361 cell line 0 and NEDD9-overexpressing cell line 0 into collagen-I matrix and into M/C in 16 hours. (**J**) Migration of control WM1361 cell line 0 and NEDD9-overexpressing cell lines 0 and 7 through Matrigel-coated Boyden chambers and migration of control WM1361 cell line 0 and NEDD9-overexpressing cell line 0 through collagen-I-coated chambers in 16 hours. (**K**) Confocal microscopy z-stack images of control WM1361 cell line 0 and NEDD9-overexpressing cell line 0 after 16 hours of invasion into M/C. Scale bar: 50 µm. (**L**) Percentage elongated cells that have invaded the M/C after 16 hours; values are means ± s.e.m., $n=3$. (**M**) Invasion index of NEDD9 siRNA (Q4, siSP)-transfected SBCL2 cells into M/C in 16 hours; knockdowns were assessed by immunoblotting; values are means ± s.e.m., $n=3$. (**N**) Invasion index of NEDD9 siRNA (siSP)-transfected SKMEL28 cells into M/C in 16 hours; knockdowns were assessed by qPCR; values are means ± s.e.m., $n=3$. *$P\leq0.05$; **$P\leq0.01$; NS, not significant.

### Integrin β3 is required for NEDD9-driven signalling

Elongated, mesenchymal-type migration has been shown to be more reliant on integrin signalling than rounded, amoeboid migration (Friedl and Wolf, 2010). The Rac GEF DOCK1, which is closely related to DOCK3, is known to be activated through integrin-mediated signalling that involves p130Cas, which is closely related to NEDD9 (Kiyokawa et al., 1998b; Smith et al., 2008). We therefore assessed whether NEDD9 signalling requires integrins. We tested blocking antibodies against integrins to see if they reversed the effect of NEDD9 overexpression on cell

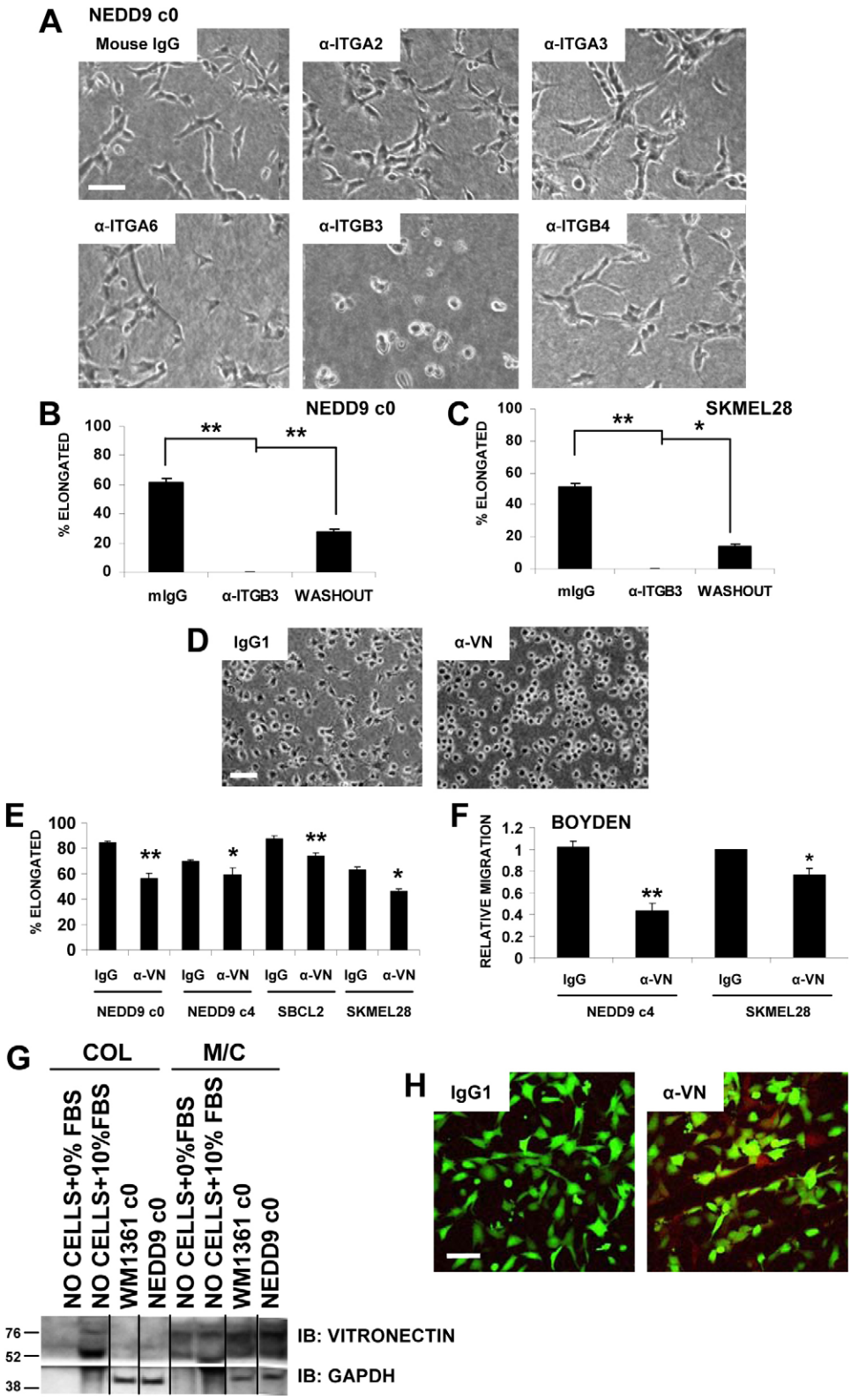


**Fig. 2. integrin β3 is required for NEDD9-driven signalling.** (**A**) Images of WM1361 NEDD9-overexpressing cell line 0 plated on serum-free M/C with integrin blocking antibodies 2 hours post plating. Scale bar: 100 µm. (**B**) Percentage of elongated cells 2 hours after plating of NEDD9-overexpressing cell line 0 on serum-free M/C with integrin β3 blocking antibody BV4; values are means ± s.e.m., $n=3$. (**C**) Percentage of elongated cells 2 hours following plating of SKMEL28 cells on serum-free M/C with integrin-β3-blocking antibody BV4; values are means ± s.e.m., $n=3$. (**D**) Images of NEDD9-overexpressing cell line 0 plated on serum-free M/C with vitronectin-blocking antibody 2 hours post plating. Scale bar: 100 µm. (**E**) Percentage of elongated cells 2 hours after plating of NEDD9-overexpressing cell lines 0, 4, SBCL2 and SKMEL28 cells on serum-free M/C with vitronectin-blocking antibody; values are means ± s.e.m., $n=3$. (**F**) Migration of NEDD9-overexpressing cell line 4 and SKMEL28 through Matrigel-coated Boyden chambers in the presence of vitronectin-blocking antibody in 16 hours; values are means ± s.e.m., $n=3$. (**G**) Vitronectin is present in Matrigel not collagen-I. Immunoblot of vitronectin under various matrix conditions (collagen-I or M/C), cell conditions (with or without cells, WM1361 cell line 0 or NEDD9-overexpressing cell line 0), and serum conditions (serum-free or 10% FBS). (**H**) Vitronectin is present in M/C. Immunofluorescence of vitronectin (red) 16 hours post plating NEDD9-overexpressing cell line 0 cells (green) on M/C in the absence of serum. Scale bar: 100 µm. *$P\leq0.05$; **$P\leq0.01$.

elongation (antibodies listed in supplementary material Table S1). Strikingly, integrin β3 (ITGB3)-blocking antibody BV4 reversed NEDD9-driven cell elongation (Fig. 2A; supplementary material Fig. S2A, Movies 1,2). This effect was reversible on wash out of the antibody (Fig. 2B; supplementary material Movie 3). Similar results were seen in the elongated melanoma cell line SKMEL28 (Fig. 2C).

Integrin β3 can associate with integrins αIIB or αv (Hynes, 1992); FACS analysis showed that the melanoma cell lines expressed integrin αvβ3 but not αIIBβ3 (supplementary material Fig. S2B). A major ligand for integrin αvβ3 is vitronectin (Cheresh and Spiro, 1987); blocking antibody against vitronectin reversed NEDD9 driven elongation in several overexpressing lines (Fig. 2D,E), as well as inhibiting migration through Matrigel-coated Boyden chambers (Fig. 2F). Similar results were obtained in the elongated melanoma cell lines SKMEL28 and SBCL2 (Fig. 2E,F). These findings show that integrin αvβ3 and its ligand vitronectin are required for NEDD9-dependent elongation. Analysis of matrix and cells showed that vitronectin is contributed from Matrigel rather than the cells (Fig. 2G,H), explaining why NEDD9-driven invasion and migration was only observed when Matrigel was included as a matrix component.

### Overexpression of NEDD9 drives integrin β3 Tyr785 phosphorylation and integrin-β3–Src complex formation

Signalling by integrin β3 is known to be regulated by phosphorylation (Datta et al., 2002; Xi et al., 2006; Oxley et al., 2008). When Tyr785 in the cytoplasmic domain is unphosphorylated, calpain cleaves off the C-terminal region leading to the loss of an atypical Src binding site. Phosphorylation at Tyr785 blocks calpain-mediated cleavage and allows the formation of an integrin-β3–Src signalling complex (Xi et al., 2006; Flevaris et al., 2007). To determine if NEDD9 overexpression influences integrin β3 signalling we looked at the effect of NEDD9 overexpression on integrin β3 phosphorylation and the interaction between integrin β3 and Src. NEDD9 overexpression led to increased integrin β3 Tyr785 phosphorylation (Fig. 3A,B). Consistent with the role of Tyr785 phosphorylation in protecting the cytoplasmic tail of integrin β3 from calpain-mediated cleavage, NEDD9 overexpression led to increased formation of integrin-β3–Src complexes (Fig. 3C–E). The increased complex formation between integrin β3 and Src occurred with no overall change in Src activity, as measured by phosphorylation at Tyr416 (Fig. 3A). Interestingly, NEDD9 and its binding partner Crk,

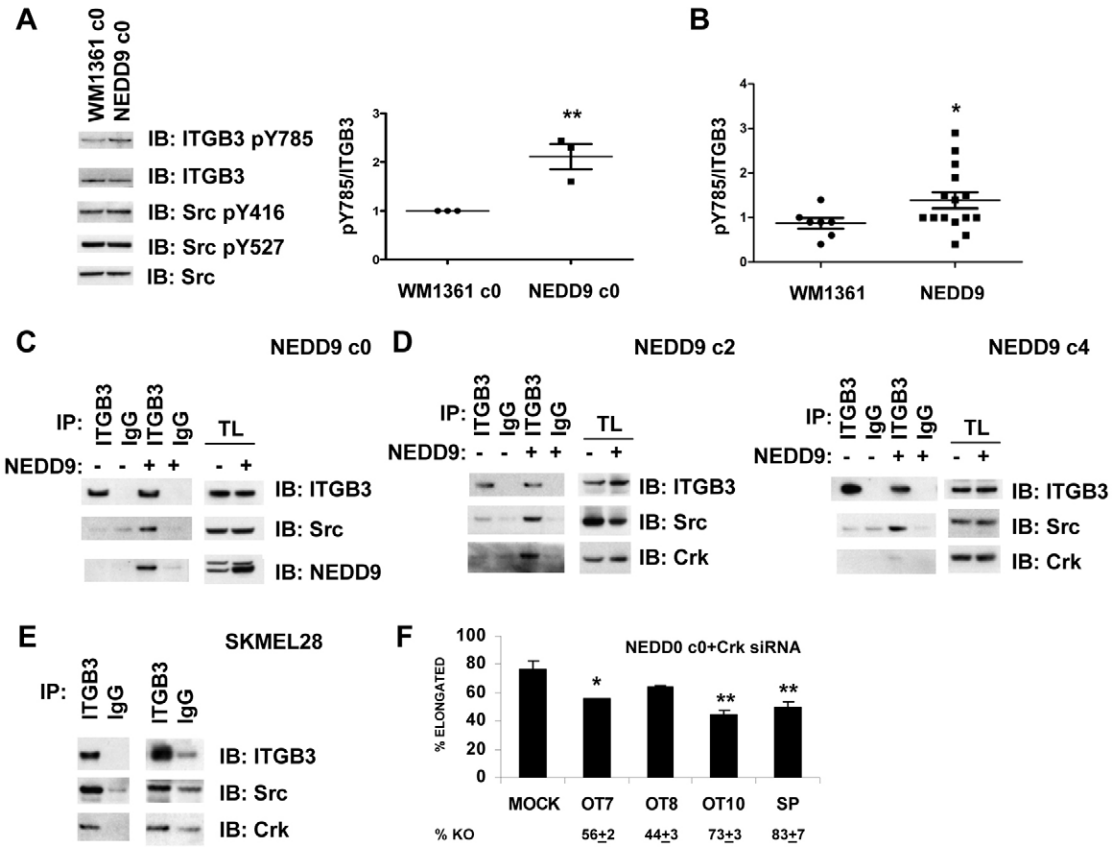


**Fig. 3. Overexpression of NEDD9 leads to integrin β3 Tyr785 phosphorylation and integrin-β3–Src complex formation.** (**A**) Immunoblot of integrin β3 Tyr785-*P* (pTyr785), Src Tyr416-*P* and Tyr527-*P* in WM1361 control cell line 0 and NEDD9-overexpressing cell line 0. One representative blot of three is shown. Scatter plot shows integrin β3 Tyr785-*P* signal normalised against integrin β3, $n=3$. (**B**) Integrin β3 Tyr785-*P* signal normalised against integrin β3 for NEDD9-overexpressing cell lines, shown as a scatter plot. Central bar indicates the mean. (**C**) Complex formation between Src and integrin β3 (ITGB3) following NEDD9 overexpression in cell line 0. (**D**) Same as C in other NEDD9-overexpressing lines (cell lines 2, 4). Crk antibody recognises both CrkI and CrkII. (**E**) Same as C in the elongated cell line SKMEL28. (**F**) Percentage of elongated cells of the NEDD9-overexpressing cell line 0 48 hours following CrkII siRNA (OT7, OT8, OT10, SP) transfection. Cell shape was quantified 2 hours post plating on serum-free M/C; percentage knockdowns were assessed by immunoblotting. Values are means ± s.e.m., $n=3$. *$P\leq0.05$; **$P\leq0.01$.

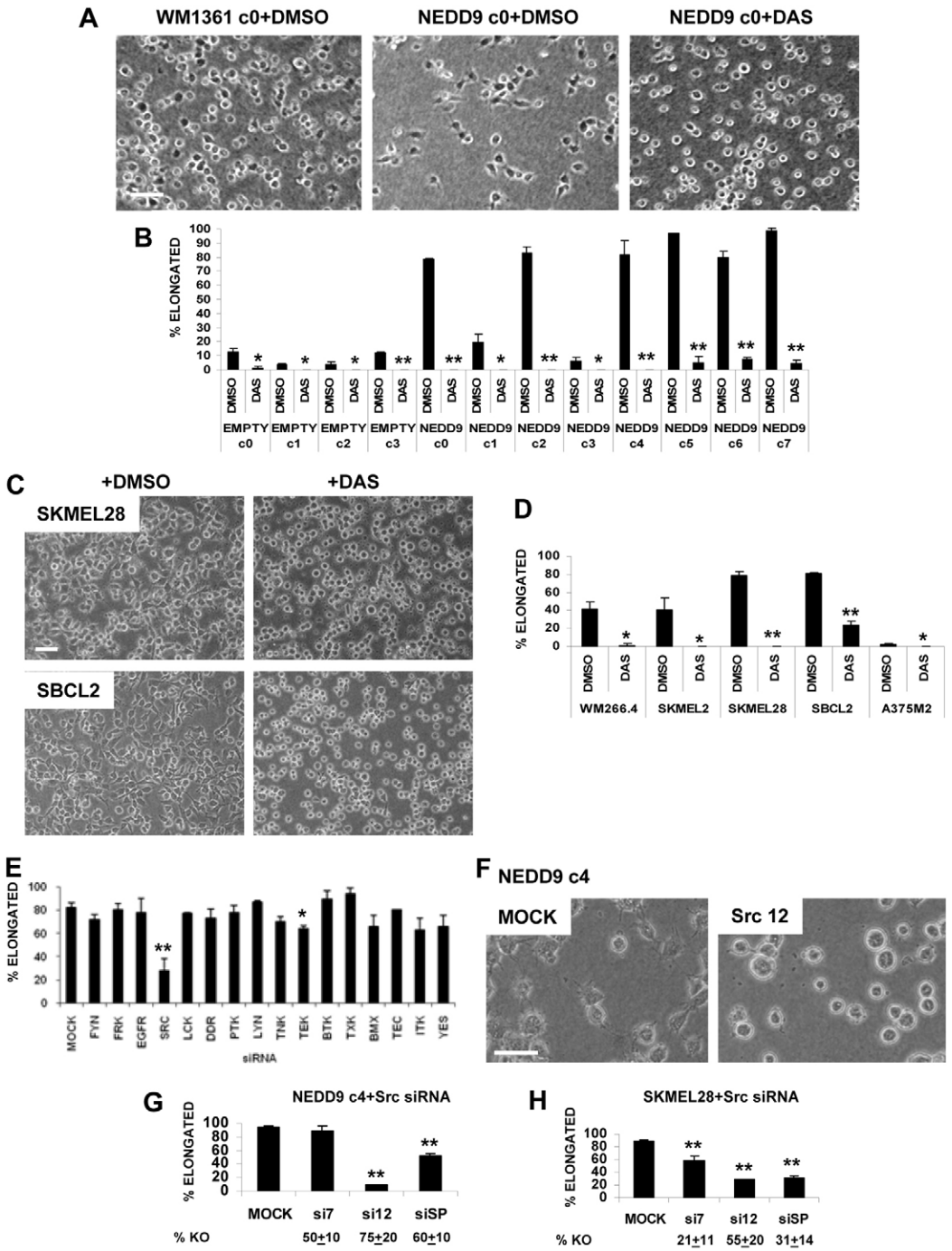


**Fig. 4. Src is required for NEDD9 signalling.** (**A**) Images of WM1361 control cell line 0 and NEDD9-overexpressing cell line 0 plated on serum-free M/C with dasatinib (DAS); 2 hours post plating. Scale bar: 100 µm. (**B**) Percentage of elongated cells following dasatinib treatment of WM1361 control and NEDD9-overexpressing cell lines 2 hours post plating on serum-free M/C. (**C**) Images of SKMEL28 and SBCL2 cells 2 hours post plating on serum-free M/C with dasatinib. Scale bar: 100 µm. (**D**) Percentage of elongated cells following dasatinib treatment of melanoma cell lines, WM266.4, SKMEL2, SKMEL28, SBCL2 and A375M2, 2 hours post plating on serum-free M/C. (**E**) siRNA knockdown of dasatinib targets in NEDD9-overexpressing cell line 0. Percentage of elongated cells 72 hours after siRNA transfection, 2 hours post plating; values are means ± s.e.m., $n=2$. (**F**) Images of NEDD9-overexpressing cell line 4, 96 hours after transfection with Src siRNA (si12) at 2 hours post plating on serum-free M/C. Scale bar: 100 µm. (**G**) Percentage of elongated cells in NEDD9-overexpressing cell line 4, 96 hours after transfection with Src siRNAs (si7, si12 or siSP) at 2 hours post plating on serum-free M/C; values are means ± s.e.m., $n=3$. Src knockdowns were assessed by immunoblotting. (**H**) Percentage of elongated cells in the SKMEL28 cell line, 96 hours after transfection with Src siRNAs (si7, si12 or siSP) 2 hours post plating; values are means ± s.e.m., $n=3$. Src knockdowns were assessed by immunoblotting; values are means ± s.e.m., $n=3$. *$P\leq0.05$; **$P\leq0.01$.

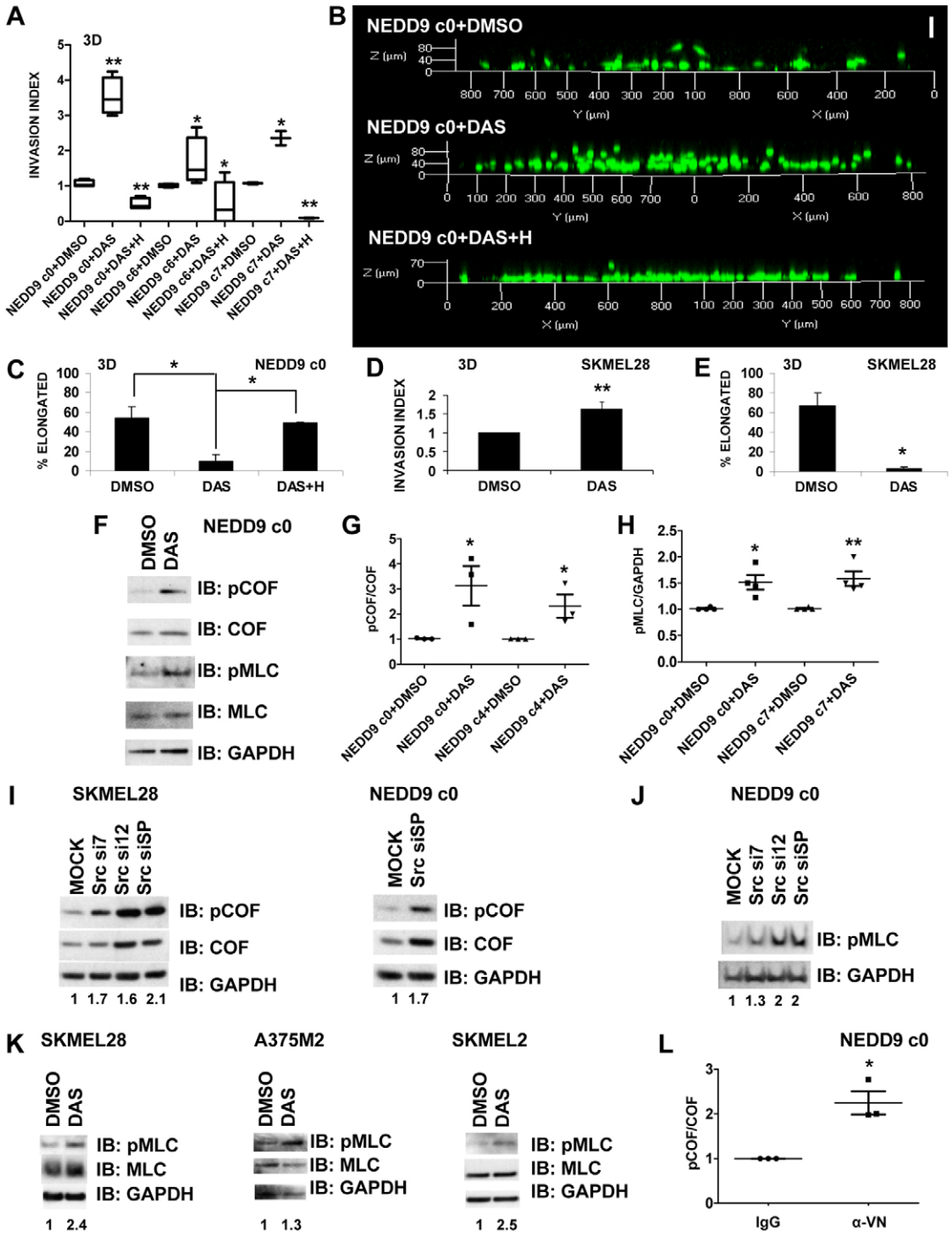


**Fig. 5. Inhibition of Src signalling promotes rounded, amoeboid invasion.** (**A**) 3D invasion into collagen-I with 5% serum of WM1361 NEDD9-overexpressing cell lines 0, 6 and 7 treated with dasatinib (DAS), $n=3$. (**B**) Images of invaded NEDD9-overexpressing cell line 0 in the presence of dasatinib or dasatinib+H-1152 after 24 hours of invasion into collagen-I with 5% serum. Scale bar: 60 μm. (**C**) Percentage of elongated invaded cells from B; values are means ± s.e.m., $n=3$. (**D**) 3D invasion of SKMEL28 into collagen-I with 5% serum, in the presence of dasatinib; values are means ± s.e.m., $n=3$. (**E**) Percentage of elongated invaded SKMEL28 cells in the presence of dasatinib; values are means ± s.e.m., $n=3$. (**F**) Immunoblot of phosphorylated cofilin (pCOF) and phosphorylated MLC (pMLC) in WM1361 NEDD9-overexpressing cell line 0 in the presence of dasatinib on serum-free M/C. The lysates were collected 2 hours post plating. A representative blot of three is shown. (**G**) Quantification of immunoblots of phosphorylated cofilin normalised against total cofilin in NEDD9-overexpressing cell lines 0 and 4, 2 hours post plating on serum-free M/C in the presence of dasatinib, expressed as a scatter plot. (**H**) Quantification of immunoblots of phosphorylated MLC in NEDD9-overexpressing cell lines 0 and 7, 2 hours post plating on serum-free M/C in presence of dasatinib, expressed as a scatter plot. (**I**) Immunoblot of phosphorylated cofilin in SKMEL28 and NEDD9-overexpressing cell line 0, 96 hours post Src siRNA (si7, si12 or siSP) transfection, 2 hours post plating on serum-free M/C. A representative immunoblot of three is shown. (**J**) Immunoblot of phosphorylated MLC in NEDD9-overexpressing cell line 0, 96 hours post Src siRNA (si7, si12 or siSP) transfection, 2 hours post plating on serum-free M/C. A representative immunoblot of three is shown. (**K**) Immunoblot of phosphorylated MLC in SKMEL28, A375M2 and SKMEL2, 2 hours post plating in serum-free M/C in the presence of dasatinib. (**L**) Quantification of immunoblots of phosphorylated cofilin after treatment of NEDD9-overexpressing cell line 0 with vitronectin-blocking antibody and plating on serum-free M/C. The lysates were collected 2 hours post plating. The results are shown as a scatter plot, $n=3$. *$P\leq0.05$; **$P\leq0.01$.

were also in this complex in the NEDD9-overexpressing WM1361 cell lines and the elongated melanoma cell line SKMEL28 (Fig. 3C–E). Crk knockdown reversed NEDD9-driven cell elongation (Fig. 3F) presumably because it is required for complex formation between NEDD9 and DOCK3 (Kiyokawa et al., 1998a; Smith et al., 2008).

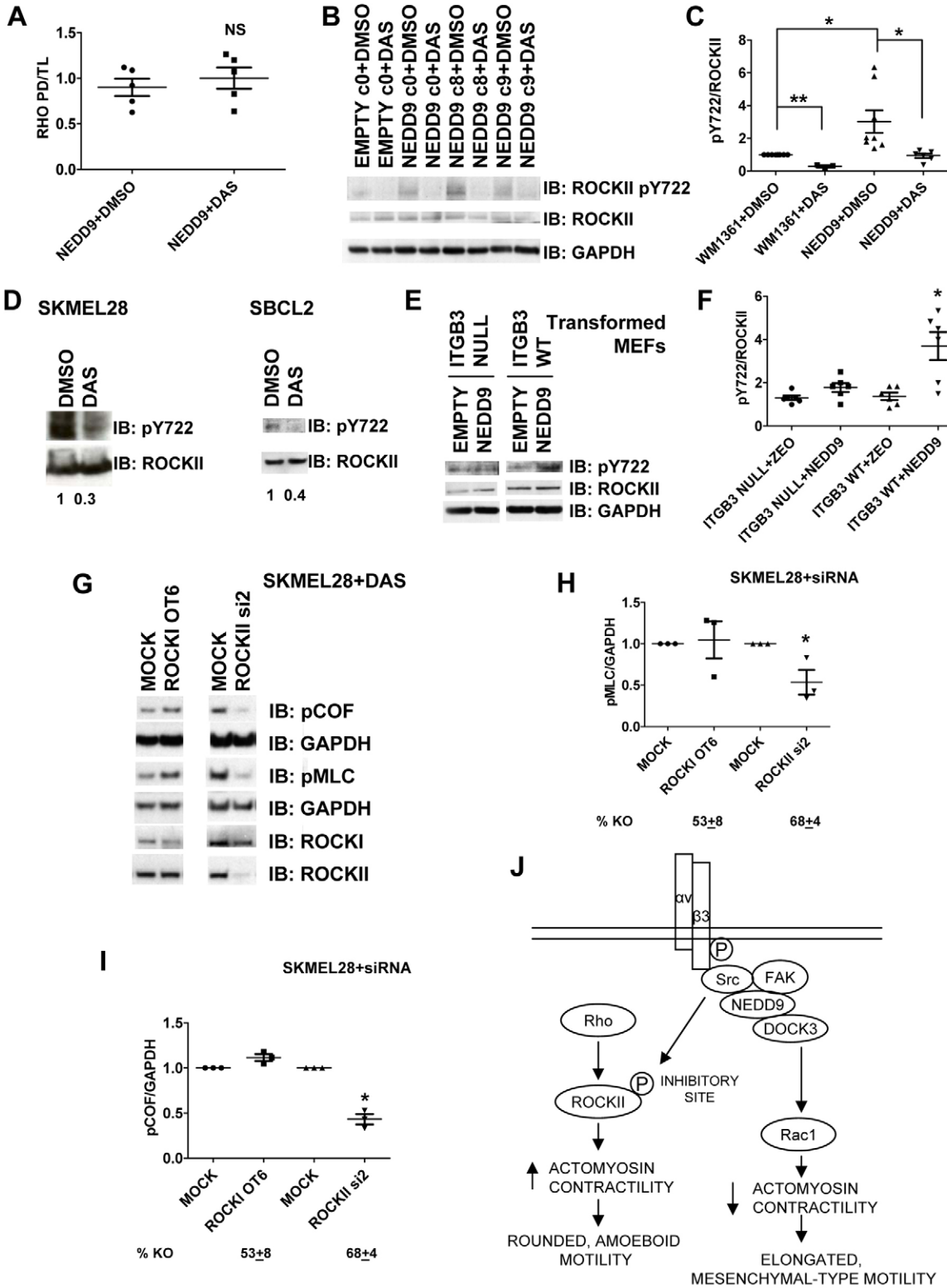


**Fig. 6.** See next page for legend.

### Src is required for NEDD9 signalling

These results suggest that Src is required for NEDD9-driven signalling. To examine the role of Src we used small molecule inhibitors of Src kinase activity. Dasatinib is a Src inhibitor effective in the subnanomolar range that acts as an ATP binding site competitor (Aleshin and Finn, 2010). Strikingly, dasatinib reversed NEDD9-driven cell elongation in all overexpression cell lines (Fig. 4A,B; for titration of dasatinib, see supplementary material Fig. S3A,B). Treatment with dasatinib reversed elongation in all human melanoma cell lines tested: WM266.4, SKMEL2, SKMEL28, SBCL2 and A375M2 (Fig. 4C,D). Because dasatinib can inhibit several kinases (Hantschel et al., 2007; Li et al., 2010) we used other inhibitors to rule out off-target effects. Treatment with the Src inhibitor PP1 blocked cell elongation (supplementary material Fig. S3C) whereas PP3, an inactive stereoisomer had no effect (supplementary material Fig. S3D). Because dasatinib inhibits the kinase activity of Abl, we used imatinib that inhibits Abl but not Src (Deininger et al., 2005); imatinib had no effect on NEDD9-driven elongation (supplementary material Fig. S3E). To extend these results we used RNA interference to knock down expression of other reported targets of dasatinib (Hantschel et al., 2007; Li et al., 2010). This analysis revealed that Src is the only target of dasatinib involved in NEDD9 signalling, as only Src knockdown reversed NEDD9-driven elongation in the WM1361 cell line overexpressing NEDD9 (Fig. 4E–G; supplementary material Fig. S3F; knockdowns in supplementary material Fig. S3G) and the elongated melanoma cell line SKMEL28 (Fig. 4H; supplementary material Fig. S3H). In the initial experiments, knockdown of TEK blocked NEDD9-driven cell elongation, but tests with four different siRNAs against TEK showed that the original result was an off-target effect (supplementary material Fig. S4A,B). These results show that Src is required for NEDD9-driven signalling.

**Fig. 6. NEDD9 overexpression induces Src-dependent ROCKII Tyr722 phosphorylation, and ROCKII knockdown decreases cofilin and MLC phosphorylation in dasatinib-treated SKMEL28 cells.** (**A**) Scatter plot of GTP-bound RhoA in dasatinib (DAS)-treated NEDD9-overexpressing lines 2 hours post plating on collagen-I with 5% serum. (**B**) Immunoblot of ROCKII Tyr722-*P* (pY722) in control WM1361 cell line 0 and NEDD9-overexpressing cell lines 0, 8 and 9, 2 hours following plating in the presence of dasatinib on serum-free M/C. A representative blot of three is shown. (**C**) Quantification of immunoblots of ROCKII Tyr722-*P* normalised against total ROCKII in control and NEDD9-overexpressing cell lines, 2 hours after plating in the presence of dasatinib on serum-free M/C, shown as scatter plot. (**D**) Immunoblot of ROCKII Tyr722-*P* normalised against total ROCKII in SKMEL28 and SBCL2, 2 hours after plating in the presence of dasatinib on serum-free M/C. A representative blot of three shown. (**E**) ROCKII Tyr722 phosphorylation requires integrin β3. Immunoblot of ROCKII Tyr722-*P* and total ROCKII in integrin-β3-null or wild-type transformed MEFs expressing dominant-negative p53, HRAS G12V, and NEDD9, 2 hours post plating on collagen-I in 5% serum. (**F**) Quantification of ROCKII Tyr722-*P* normalised against total ROCKII in integrin-β3-null or wild-type MEFs described in E. The results from three independent populations expressing NEDD9 were compiled as a scatter plot; ZEO, zeocin resistance empty vector. (**G**) Immunoblot of phosphorylated cofilin and MLC in SKMEL28 cells 48 hours post ROCKI siRNA (OT6) or ROCKII siRNA (si2) transfection, 2 hours post plating in the presence of dasatinib on collagen-I in 5% serum. A representative immunoblot of three is shown. (**H**) Quantification of immunoblots of phosphorylated MLC from G, shown as a scatter plot; $n=3$. Knockdowns were assessed by immunoblotting; values are means ± s.e.m., $n=3$. (**I**) Quantification of immunoblots of phosphorylated cofilin from G, shown as a scatter plot; $n=3$. Knockdowns were assessed by immunoblotting; values are means ± s.e.m., $n=3$. (**J**) Diagram of the relationship between key signalling molecules with respect to the mode of migration. $^{*}P\leq0.05$; $^{**}P\leq0.01$.

### Inhibition of Src signalling promotes rounded, amoeboid invasion

To investigate the role of Src in NEDD9-driven invasion we investigated the effects of Src inhibition. Interestingly, rather than blocking invasion, dasatinib treatment enhanced 3D invasion (Fig. 5A). Treatment with dasatinib also changed the mode of invasion. Dasatinib-treated NEDD9-overexpressing lines invaded as rounded, amoeboid cells rather than as elongated cells (Fig. 5B,C). This is consistent with previous reports that Src family kinase inhibitor PP2 inhibits movement of cells using mesenchymal motility but promotes movement of cells using amoeboid motility (Carragher et al., 2006). We show that increased rounded, amoeboid invasion was inhibited by the ROCK inhibitor H-1152 (Fig. 5A,B), consistent with this mode of invasion being highly dependent on Rho–ROCK signalling (Sahai and Marshall, 2003). In the elongated human melanoma cell line SKMEL28, dasatinib treatment also increased rounded, amoeboid invasion (Fig. 5D,E), which was inhibited by H-1152 (data not shown). To investigate whether inhibiting Src signalling promotes rounded, amoeboid cell migration through increased ROCK signalling, we examined the phosphorylation of MLC and cofilin. Phosphorylation of MLC and cofilin was increased by dasatinib treatment or Src knockdown (Fig. 5F–K). These data suggest NEDD9 activates Src signalling to suppress ROCK signalling and, accordingly, overexpression of NEDD9 in WM1361 cells led to decreased phosphorylation of MLC (Fig. 1D,E), whereas knockdown of NEDD9 in SKMEL2 cells increased MLC phosphorylation (supplementary material Fig. S1D,E). These findings show that NEDD9–Src signalling in elongated, mesenchymal-type invasion involves suppression of ROCK-dependent signalling. Abolition of Src signalling increases ROCK signalling and therefore leads to rounded, amoeboid invasion.

Having shown that NEDD9 overexpression results in the assembly of integrin-β3–Src complexes we investigated whether integrin β3 is required for the suppression of ROCK signalling. Similar to inhibiting Src, blocking integrin β3 signalling by using a vitronectin-blocking antibody increased phosphorylation of cofilin (Fig. 5L). Overall these results suggest that blocking NEDD9 signalling shifts the balance between Rac-dependent, elongated, mesenchymal-type movement and ROCK-dependent rounded, amoeboid cell movement.

### NEDD9 overexpression results in Src-dependent ROCKII Tyr722 phosphorylation

The results described above show that NEDD9 signalling through Src suppresses ROCK signalling. Because we have shown that NEDD9 overexpression does not decrease RhoA–GTP levels (Fig. 1F), this suggests that Src must act downstream of Rho activation. Furthermore, whereas dasatinib treatment led to increased ROCK signalling it did not increase RhoA activation (Fig. 6A). Src has been recently reported to phosphorylate ROCKII on Tyr722 to decouple it from RhoA and block ROCKII signalling (Lee, H. H. et al., 2010). Therefore, we tested whether ROCKII Tyr722 phosphorylation was increased through NEDD9

overexpression. Strikingly, ROCKII Tyr722 phosphorylation was increased in several NEDD9-overexpressing cell lines, and was inhibited by dasatinib treatment (Fig. 6B,C). We also found that in elongated melanoma cell lines, SKMEL28 and SBCL2, dasatinib decreased Tyr722 phosphorylation (Fig. 6D).

To determine whether NEDD9-driven ROCKII phosphorylation is dependent on integrin β3 we used integrin-β3-null MEFs, transformed by dominant-negative p53 and HRAS G12V. NEDD9 overexpression increased ROCKII Tyr722 phosphorylation in transformed MEFs derived from wild-type controls but not in integrin-β3-null MEFs (Fig. 6E,F; supplementary material Fig. S5). Thus Src-dependent Tyr722 phosphorylation of ROCKII in cells overexpressing NEDD9 requires integrin β3.

These results suggest that the increased ROCK signalling seen after dasatinib treatment depends on ROCKII rather than ROCKI. To assess the contribution of ROCKII to the dasatinib-dependent increase in actomyosin contractility, ROCKI and II were knocked down by siRNAs in the elongated melanoma cell line SKMEL28. Although ROCKI knockdown had no effect on the dasatinib-induced increase in phosphorylation of MLC, ROCKII knockdown significantly decreased phosphorylation (Fig. 6G,H; supplementary material Fig. S6A). Similar results were found for phosphorylation of cofilin in response to dasatinib treatment (Fig. 6G,I; supplementary material Fig. S6B). These findings suggest that NEDD9 and Src act to downregulate ROCK signalling specifically by acting on ROCKII.

## Discussion

In this study we showed that integrin β3 and its ligand vitronectin are required for NEDD9-driven cell elongation and invasion. NEDD9 overexpression leads to increased phosphorylation of Tyr785 in the cytoplasmic tail of integrin β3 and the assembly of a signalling complex containing integrin β3, Src, FAK and NEDD9 (Fig. 6J). NEDD9 is known to bind to the C-terminus of FAK through its SH3 domain (Minegishi et al., 1996; Hanks and Polte, 1997). However, NEDD9 overexpression does not seem to increase the activating phosphorylation on Src at Tyr416, thus the role for integrin β3 appears to be to assemble a signalling complex containing Src. Interestingly the kinase responsible for phosphorylating integrin β3 Tyr785 in NEDD9-overexpressing cells does not seem to be Src itself, because dasatinib treatment had no effect on integrin β3 Tyr785 phosphorylation (supplementary material Fig. S7). Increased activity of Src and elevated levels of integrin αvβ3 are often found in the same tumour type (Albelda, 1990; Felding-Habermann et al., 1992; Huveneers et al., 2007; Lee, J. H. et al., 2010) and recent evidence from in vivo studies and patient material indicate that this complex plays a role in human tumour progression (Huveneers and Danen, 2010). Our findings suggest that NEDD9 only promotes motility in specific environments where there are ligands for integrin αvβ3, such as vitronectin.

Kim et al., who first identified the role of NEDD9 in melanoma metastasis, made the observation that NEDD9 overexpression leads to elevated FAK activation (Kim et al., 2006). This is somewhat surprising on a linear model of signalling where a Cas family member would be expected to be downstream of FAK (McLean et al., 2005), and because FAK overexpression leads to increased NEDD9 phosphorylation (Natarajan et al., 2006). However, the observations made here that NEDD9 signalling depends on integrin αvβ3 and leads to assembly of an integrin β3 signalling complex provides a rationalisation of why NEDD9 overexpression leads to increased activation of FAK.

Rac and Rho have opposing roles in different modes of tumour cell motility, and changing the activity of one signalling pathway can change the mode of movement (Sanz-Moreno et al., 2008). For rounded, amoeboid movement, Rho–ROCK activity must be high to generate high actomyosin contractility, and Rac activity low because Rac can suppress actomyosin contractility through WAVE2 (Sanz-Moreno et al., 2008). We have shown that Rac activity is kept low for rounded, amoeboid movement through Rho–ROCK signalling activating a Rac GAP, ARHGAP22 (Sanz-Moreno et al., 2008). Conversely, in elongated, mesenchymal-type movement, Rac activity is elevated and Rho–ROCK signalling activity must be kept low to prevent the generation of too much actomyosin contractility. An important finding from our studies is that NEDD9 overexpression modulates Src signalling to oppose Rho–ROCKII signalling that could drive high levels of actomyosin contractility. NEDD9–Src signalling opposes Rho–ROCKII signalling not by decreasing Rho activation but by Src-dependent phosphorylation of the negative regulatory Tyr722 site on ROCKII (Lee, H. H. et al., 2010). Thus NEDD9 signalling acts as an accelerator of elongated, mesenchymal-type movement by activating the Rac pathway and puts a brake on pathways driving rounded, amoeboid movement by suppressing ROCKII activity.

Together with our previous work demonstrating a NEDD9–DOCK3 complex (Sanz-Moreno et al., 2008) these studies demonstrate that there are at least two consequences of NEDD9 overexpression: Rac activation and Src signalling to inhibit ROCKII. Both of these signalling events contribute to elongated, mesenchymal-type movement.

The key role of Src for NEDD9-driven promotion of elongated, mesenchymal-type cell movement and suppression of rounded, amoeboid movement is demonstrated by the observation that Src inhibitors such as dasatinib lead to cells adopting amoeboid invasion. Given that dasatinib is being assessed for clinical use in metastatic melanoma (Eustace et al., 2008), our results raise the prospect that inhibition of Src might promote the rounded, amoeboid mode of tumour invasion. The observation that dasatinib blocks elongated, mesenchymal-type invasion, while promoting rounded, amoeboid invasion, indicates that combination therapy to concurrently block different modes of motility might be desirable, for example, a Src inhibitor with a ROCK inhibitor.

## Materials and Methods

### Antibodies

The following antibodies were used: mIgG (Abcam, ab18448), rIgG (R&D, AB-105-C), gIgG (R&D, AB-108-C), 4G10 Platinum (Millipore, 05-1050), anti-cofilin [Cell Signaling Technology (CST), 3312S), anti-phosphorylated cofilin (Ser3) (CST, 3311S), anti-Crk (BD 610036; Epitomics 1779-1), ECL rabbit IgG (GE Amersham, NA934-100UL), ECL mouse IgG (GE Amersham, NA931-100UL), anti-GAPDH (Stratech, NB300-221), anti-integrin-αvβ3 (Millipore, MAB1976Z clone LM609) anti-integrin-β3 (CST 4702, Abcam, ab7167 clone BV4), anti-integrin-β3 Y785-*P* (Abcam, ab7167), anti-integrin-β3 Y773-*P* (Abcam, ab5190), 10E5 antibody (kindly provided by Barry Coller, Rockefeller University, New York, USA), anti-MLC (Santa Cruz sc15370; Sigma M4401), anti-phosphorylated MLC Thr18/Ser19 (CST, 3674S), anti-NEDD9 (Abcam, ab37161, ab18056 clone 2G9), anti-Rac1 (Millipore, 05–389 clone 23A8), anti-ROCKII (Santa Cruz, sc1851c20; BD, 610624), anti-ROCKII Y722-*P* (kindly provided by Hsiao-Hui Lee and Zee-Fen Chang, National Yang-Ming University, Taipei, Taiwan), anti-Src (CST, 2110 clone L4A1; CST 2109), anti-Src Y416-*P* (CST, 2101S), anti-Src Y527-*P* (CST, 2105), anti-vitronectin (Abcam, ab7165, clone BV1; Millipore, MAB1945 clone BV2) and integrin blocking antibodies as shown in supplementary material Table S1.

### Plasmids and reagents

LZRSpBMN-Z-delta-NEDD9 was from Linda Chin (Dana Farber Cancer Institute, MA, USA) and empty vector control was cloned by removing NEDD9. Sure Silencing shRNA plasmids for NEDD9 were from SuperArray (KH18884P). Recombinant glutathione S-transferase-conjugated Rhotekin-RBD and PAK-CRIB were expressed from pGEX-Rhotekin and pGEX-CRIB. Reagents used were: H1152 (at 5 μM; Calbiochem, Merck); PP1, PP3 (Calbiochem, Merck); dasatinib (Sequoia Research SRP00930d); PF-562271 (Symansis); and imatinib (Don White, ICR, London, UK).

### Cell culture

Human melanoma cell lines SKMEL2, SKEML28, A375M2, SBCL2 and WM1361 were obtained from Richard Marais (ICR, London, UK). WM1361 was transfected with GFP empty vector or NEDD9 GFP vector to make control and NEDD9-overexpressing cell lines. Each cell line was generated from pools of clones. Cells selected by FACS or puromycin resistance had a higher proportion of round cells compared with the parental cell line. Integrin β3 knockout MEFs were isolated by Afsan McCarthy (ICR, London, UK). Cells were maintained in DMEM or RPMI with 10% FBS (foetal bovine serum, PAA), 100 μg/ml streptomycin and 60 μg/ml penicillin, and kept at 37℃ in 10% $CO_2$. Plasmid transfections were performed with Lipofectamine 2000 (Invitrogen) according to manufacturer's instructions. Stable cell lines were selected with G418 at 100 mg/ml or puromycin at 2.5 μg/ml (Calbiochem).

### Cell culture on thick deformable matrices

Bovine skin collagen-I (Nutacon PureCol 5005-B, pepsinised, telopeptide free) was prepared at 1.8 mg/ml dilution in DMEM (free of Phenol Red and serum) according to the manufacturer's protocol. M/C was made using growth-factor-reduced Matrigel (BD 356231) at 1.8 mg/ml and collagen-I at 1.9 mg/ml. 300 μl M/C was placed in wells of 24-well plates, 700 μl in 12-well plates and 2 ml in six-well plates and polymerised at 37℃ in 10% $CO_2$ for 3–6 hours. Cells were seeded on top of matrix in medium (serum-free unless indicated) and allowed to adhere for 2 hours, imaged and lysates collected or time-lapse imaged for 16–48 hours. The earliest time point at which difference in cell morphology was observed was 2 hours. Except for immunoprecipitations, all cell imaging, immunoblotting and pulldown assays were performed on cells cultured on a thick layer of collagen-I or a mixture of collagen-I and growth-factor-reduced Matrigel (M/C).

### siRNA transfections

siRNA oligonucleotide duplexes were purchased from Dharmacon (Thermo Scientific). For transfection, 300,000 cells were plated in six-well plates and transfected with 20 nM SMART pool or individual oligonucleotides with Optimem-I (Qiagen) and Lipofectamine 2000. Cells were re-plated on M/C without serum or collagen-I with 5% serum and analyzed 2 hours post plating. siRNA sequences are listed in supplementary material Table S2.

### qPCR

Total cellular RNA was isolated from cultured cells using RNAeasy Mini kit (Qiagen) according to the manufacturer's instructions. qRT-PCR amplifications were performed using Brilliant II SYBR Green qRT-PCR Master Mix kit (Stratagene). A standard curve was constructed using a range from 0.01 to 10 ng RNA for each set of primers used. Relative quantification was performed using the ΔΔCt method. All primers used were Quantitect SYBR Green primer assays (Qiagen). Reactions were performed in triplicate in 50 μl volumes containing 25 μl 2× Brilliant II mastermix, 5 μl 10× Quantitect SYBR Green primer, 1 μl RT-RNase-block enzyme mixture (Stratagene), and the appropriate amount of RNA, with the remaining volume made up with nuclease-free water (Ambion). PCR was performed in an Applied Biosystems 7900 HT Fast Real-Time PCR cycler. Fluorescence data were analysed using Applied Biosystems SDS software.

### Immunoprecipitation and immunoblotting

For immunoprecipitations, cells were plated on plastic in serum-free medium and allowed to adhere for 2 hours at 37℃ in 10% $CO_2$. Cells were stimulated with 10% serum for 15–30 minutes at 37℃ in 10% $CO_2$, lysed in MS buffer [0.5% NP-40, 150 mM NaCl, 50 mM Tris-HCl pH 7.5, 5 mM NaF, 0.2 mM sodium vanadate, 10 mM NaPPi (Sigma, S6422-100G), 1 mM PMSF (Fluka, 78830, diluted in ethanol), 51 μM β-glycerophosphate (Acros Organics, 410991000), 10 nM okadaic acid (Sigma, O9381), 10 nM caliculyn A (Calbiochem, 208851 diluted in ethanol) and complete EDTA-free protease inhibitor (Roche, 11-873-580-001)]. Lysates were collected, vortexed for 30 seconds, kept on ice for 10 minutes, centrifuged at 13,000 rpm for 10 minutes, pre-cleared with IgG for 15 minutes, and protein G agarose for 15 minutes, on a rotating wheel. Total lysate sample was collected and the rest of the lysate used for immunoprecipitations. Immunoprecipitations were carried out at 4℃ for 2–3 hours on a rotating wheel. Immune complexes were precipitated with 25 μl protein G agarose beads (Pierce Thermo, 20399) for 15 minutes at 4℃. After precipitation, beads were washed three times in 500 μl MS buffer, and once with 0.5 M LiCl in 100 mM Tris pH 7.4, and resuspended in NuPage sample buffer with reducing agent (Invitrogen, NP0007, NP0004) at 70℃ for 10 minutes. All normalisations were done against GAPDH. For immunoblotting total lysates, whole-cell extracts from matrices were harvested in Laemmli sample buffer and sonicated for 15 seconds prior to centrifugation at 13,000 rpm for 30 minutes. Loading dye was added and the mixture was boiled at 100℃ for 5 minutes. Immunocomplexes were visualized by the ECL Plus Western Blotting Detection System (GE Healthcare, Amersham) with horseradish peroxidase-conjugated secondary antibodies.

### Pulldown assays

Pulldown assays were performed as described by Sahai and Marshall (Sahai and Marshall, 2002). Extracts were derived from cells 2 hours post plating on a thick collagen matrix in 5% serum.

### Blocking antibody experiments

Antibodies were dialyzed to remove sodium azide. Cells were plated on serum-free M/C with anti-vitronectin antibody BV1/isotype-matched IgG (20 μg/ml) or integrin-β3-blocking antibody BV4/isotype matched IgG (25–40 μg/ml), and analysed 2 hours post plating.

### Boyden chamber assays

Transwell plates of 6.5 mm diameter with an 8 μm pore polycarbonate membrane inserts (Fisher Scientific TKT-525-110 X) were used. The matrix mix composition for collagen-I coat was: 30 μl 3.2 mg/ml collagen-I, 200 μl 5× DMEM (made in house), 740 μl water, 30 μl 0.1 M NaOH. The Matrigel coat consisted of: 12.3 μl 8.1 mg/ml growth-factor-reduced Matrigel, 200 μl 5× DMEM, 788 μl water. 900 μl of matrix coat was put in the well and 100 ml in the insert, and left overnight at 4℃. A stock suspension of 50,000 cells in 100 μl serum-free medium was prepared. To each well 100 μl cells in medium was added. Cells were allowed to attach for 45 minutes, 1 ml 5% FBS medium was added to the bottom, and incubated at 37℃ in 10% $CO_2$. The next day, inserts were placed in 1 ml PBS at room temperature (RT) for 10 minutes, then in 1 ml trypsin at 37℃ in 10% $CO_2$ for 10 minutes. Plates were placed on a plate shaker (at 1050 rpm) at RT for 10 minutes. Once cells detached from the membrane, 500 μl 10% medium was added to each well, the cells were resuspended by thorough pipetting, and then counted using a cell counter.

### Invasion assays

$2.5 \times 10^4$ cells were suspended in 500 μl of serum-free matrix composed of 1.7 mg/ml growth-factor-reduced Matrigel and 1.8 mg/ml collagen-I or collagen I only at 2.2 mg/ml until the cells reached a density of 5000 cells/100 ml. 100 μl aliquots were dispensed into 96-well ViewPlates (Perkin-Elmer 6005182) coated with bovine serum albumin. Plates were centrifuged at 1000 rpm at 4℃ and incubated at 37℃ in 10% $CO_2$ for 1.5 hours. Once polymerised, 5% serum was added with inhibitors where indicated. Where inhibitors were used, they were also mixed into the matrix before polymerisation. After 16–24 hours incubation, cells were fixed in 4% formaldehyde and stained with 5 mg/ml Hoechst 33258 (Molecular Probes, Invitrogen). Confocal Z slices were collected from each well at 50 μm and 3 μm (bottom of well) with an INCELL3000 high-content microscope. Nuclear staining was quantified with INCELL3000 software with the Object Intensity module. Samples were run in quadruplicate and averaged. The invasion index was calculated as the number of cells at 50 μm divided by the total number of cells. Data are presented as invasion index relative to that of mock-transfected or vehicle-treated cells. For the 3D imaging of invaded cells, cells were prepared in the same way using double the number of cells and matrix, and Ibidi 89626 μ-Plates. Sequential Z sections of embedded cells were obtained by imaging GFP-expressing cells with a Zeiss LSM710 confocal microscope and reconstructions were made with ZEN software (Zeiss). For evaluation of the percentage of elongated cells invading, a cell was considered elongated when its longest dimension was twice the shortest and when it showed at least one protrusion. Values are expressed as invasion index with mock or control or isotype antibody set as 1.

### Microscopy

Static phase contrast images were obtained using a Nikon Digital Site DS-4 microscope camera workstation attached to a Nikon TS100 inverted phase-contrast microscope with a Nikon LW 20× objective (0.4 NA). Images were processed for contrast and brightness using Adobe Photoshop v 7.0 (Adobe Systems UK). Multi-site time-lapse video microscopy was performed in a humidified, $CO_2$-equilibrated chamber at 37℃ using a Nikon TE2000 inverted phase contrast microscope in conjunction with either Hamamatsu Orca-ER or C9100EM-CCD digital cameras, equipped with motorised stage, focus and shutter systems (Prior Scientific Instruments, Ltd) all controlled by Simple PCI AIC (v. 6.5) acquisition software (Compix Imaging Systems). Cells were imaged using a Nikon PlanFluor 10× (0.3 NA) or PlanFluor ELWD 20× (0.45 NA) objectives for 24–48 hours at

a rate of 1 frame per site per 10 minutes. Movies were exported from Simple PCI software as uncompressed. AVI files with a frame rate of 15 frames/second.

### Vitronectin immunofluorescence

100 µl M/C was plated in an Ibidi 89626 µ-Plate and incubated for 4.5 hours at 37℃ in 10% $CO_2$. $1.5 \times 10^4$ cells were plated serum-free and incubated for 20 hours at 37℃ in 10% $CO_2$. 0.1 ml 4% formaldehyde was added for 15 minutes at room temperature (RT), and washed twice in PBS. 0.1 ml 0.2% Triton X-100 was added for 30 minutes at RT and washed three times in PBS. Vitronectin antibody (ab7165, 0.1 mg/ml, 1:10)was added in 100 µl PBS for 2 hours at 37℃ in 10% $CO_2$ and washed twice in PBS. APC-rat anti-mouse IgG (BD550874, 1:300) was added in 0.5% BSA, 0.1% Triton X-100 for 1 hour at 37℃ in 10% CO2 and washed twice in PBS. The matrix was placed on a MatTek glass dish (P35G-1.5-1.0-c 3-mm dish no.15 coverglass 0.16-0.19 mm), and imaged on the Zeiss LSM710 microscope. All images were taken at the same acquisition conditions and identically processed.

### NEDD9 tissue microarray immunohistochemistry

All procedures using human tissues were approved by the Ethics Committees of the Institute of Cancer Research and the Royal Marsden Hospital Foundation Trust, in accordance with the Human Tissue Act 2004 (chapter 30). The high density melanoma tissue microarray (Tissue Microarray ME1004) was purchased from Biomax (Rockville, MD), and contained multiple primary, malignant and metastatic melanoma samples collected with full donor consent under Institutional Review Board (IRB)- and Health Insurance Portability and Accountability Act of 1996 (HIPPA)-approved protocols. Staining was done as follows: citrate buffer pH 6.0 was added, microwaved at full power for 18 minutes and cooled for 20 minutes at RT. Serum-free protein block was performed for 5 minutes, and NEDD9 Abcam 2G9 antibody (1:75) was added for 60 minutes. Polymer - Dako Envision mouse was added for 30 minutes, and the colour substrate Diaminobenzidene (Dako, 1:10) was added for 10 minutes with a light Haematoxylin nuclear counterstain. Cell shape was assessed following the method of Viros et al. (Viros et al., 2008). Each core (diameter 1 mm) was visually assessed in its entirety at 20× and graded from 0 to 3: round cells (long and short diameters approximately equal) classified as 0; ovoid cells (long diameter approximately one-third greater than the short diameter) as 1; elongated (long diameter between one-third and two times longer than the short diameter) as 2; and spindle (long diameter two times the short diameter) as 3.

### Statistical analysis

Student's *t*-test was performed to determine whether the difference between two groups was significant for quantifications of Rac activation, protein phosphorylation, percentage of elongated cells and invasion index. When more than two groups were analysed, one-way analysis of variance (ANOVA) was used. $P \leq 0.05$ was considered to be significant.

Linear regression analysis was performed for the correlation of cell shape and NEDD9 staining intensity, using Microsoft Excel. Linear equation and correlation coefficients ($R^2$ values) are shown.

## Acknowledgements

We thank Hugh Paterson for advice on microscopy, Amaya Viros for advice on histopathology, Eric Ward for histological preparation and Afshan McCarthy for assistance with MEFs.

## Funding

This work was supported by Cancer Research UK [grant number C107/A10433 to C.J.M.]; and the Institute of Cancer Research [grant number C33043/A12065 to V.S.M.]. Deposited in PMC for release after 6 months.

Supplementary material available online at
http://jcs.biologists.org/lookup/suppl/doi:10.1242/jcs.101444/-/DC1

## References

**Albelda, S. M.** (1990). Integrin distribution in malignant melanoma: association of the [beta]3 subunit with tumor progression. *Cancer Res.* **50**, 6757-6764.

**Aleshin, A. and Finn, R. S.** (2010). SRC: a century of science brought to the clinic. *Neoplasia* **12**, 599-607.

**Astier, A., Manie, S. N., Avraham, H., Hirai, H., Law, S. F., Zhang, Y., Golemis, E. A., Fu, Y., Druker, B. J., Haghayeghi, N. et al.** (1997). The related adhesion focal tyrosine kinase differentially phosphorylates p130Cas and the Cas-like protein, p105HEF1. *J. Biol. Chem.* **272**, 19719-19724.

**Carragher, N. O., Walker, S. M., Scott Carragher, L. A., Harris, F., Sawyer, T. K., Brunton, V. G., Ozanne, B. W. and Frame, M. C.** (2006). Calpain 2 and Src dependence distinguishes mesenchymal and amoeboid modes of tumour cell invasion: a link to integrin function. *Oncogene* **25**, 5726-5740.

**Cheresh, D. A. and Spiro, R. C.** (1987). Biosynthetic and functional properties of an Arg-Gly-Asp-directed receptor involved in human melanoma cell attachment to vitronectin, fibrinogen, and von Willebrand factor. *J. Biol. Chem.* **262**, 17703-17711.

**Datta, A., Huber, F. and Boettiger, D.** (2002). Phosphorylation of beta3 integrin controls ligand binding strength. *J. Biol. Chem.* **277**, 3943-3949.

**Deininger, M., Buchdunger, E. and Druker, B. J.** (2005). The development of imatinib as a therapeutic agent for chronic myeloid leukemia. *Blood* **105**, 2640-2653.

**Donninger, H., Bonome, T., Radonovich, M., Pise-Masison, C. A., Brady, J., Shih, J., Barrett, J. C. and Birrer, M. J.** (2004). Whole genome expression profiling of advance stage papillary serous ovarian cancer reveals activated pathways. *Oncogene* **23**, 8065-8077.

**Eustace, A. J., Crown, J., Clynes, M. and O'Donovan, N.** (2008). Preclinical evaluation of dasatinib, a potent Src kinase inhibitor, in melanoma cell lines. *J. Transl. Med.* **6**, 53.

**Felding-Habermann, B., Mueller, B. M., Romerdahl, C. A. and Cheresh, D. A.** (1992). Involvement of integrin alpha V gene expression in human melanoma tumorigenicity. *J. Clin. Invest.* **89**, 2018-2022.

**Flevaris, P., Stojanovic, A., Gong, H., Chishti, A., Welch, E. and Du, X.** (2007). A molecular switch that controls cell spreading and retraction. *J. Cell Biol.* **179**, 553-565.

**Friedl, P. and Wolf, K.** (2010). Plasticity of cell migration: a multiscale tuning model. *J. Exp. Med.* **207**, 11-19.

**Hanks, S. K. and Polte, T. R.** (1997). Signaling through focal adhesion kinase. *BioEssays* **19**, 137-145.

**Hantschel, O., Rix, U., Schmidt, U., Burckstummer, T., Kneidinger, M., Schutze, G., Colinge, J., Bennett, K. L., Ellmeier, W., Valent, P. et al.** (2007). The Btk tyrosine kinase is a major target of the Bcr-Abl inhibitor dasatinib. *Proc. Natl. Acad. Sci. USA* **104**, 13283-13288.

**Harte, M. T., Hildebrand, J. D., Burnham, M. R., Bouton, A. H. and Parsons, J. T.** (1996). p130Cas, a substrate associated with v-Src and v-Crk, localizes to focal adhesions and binds to focal adhesion kinase. *J. Biol. Chem.* **271**, 13649-13655.

**Huveneers, S. and Danen, E. H.** (2010). The interaction of SRC kinase with beta3 integrin tails: a potential therapeutic target in thrombosis and cancer. *ScientificWorldJournal* **10**, 1100-1105.

**Huveneers, S., van den Bout, I., Sonneveld, P., Sancho, A., Sonnenberg, A. and Danen, E. H.** (2007). Integrin alpha v beta 3 controls activity and oncogenic potential of primed c-Src. *Cancer Res.* **67**, 2693-2700.

**Hynes, R. O.** (1992). Integrins: versatility, modulation, and signaling in cell adhesion. *Cell* **69**, 11-25.

**Ishino, M., Ohba, T., Sasaki, H. and Sasaki, T.** (1995). Molecular cloning of a cDNA encoding a phosphoprotein, Efs, which contains a Src homology 3 domain and associates with Fyn. *Oncogene* **11**, 2331-2338.

**Iwata, S., Souta-Kuribara, A., Yamakawa, A., Sasaki, T., Shimizu, T., Hosono, O., Kawasaki, H., Tanaka, H., Dang, N. H., Watanabe, T. et al.** (2005). HTLV-I Tax induces and associates with Crk-associated substrate lymphocyte type (Cas-L). *Oncogene* **24**, 1262-1271.

**Izumchenko, E., Singh, M. K., Plotnikova, O. V., Tikhmyanova, N., Little, J. L., Serebriiskii, I. G., Seo, S., Kurokawa, M., Egleston, B. L., Klein-Szanto, A. et al.** (2009). NEDD9 promotes oncogenic signaling in mammary tumor development. *Cancer Res.* **69**, 7198-7206.

**Kim, M., Gans, J. D., Nogueira, C., Wang, A., Paik, J. H., Feng, B., Brennan, C., Hahn, W. C., Cordon-Cardo, C., Wagner, S. N. et al.** (2006). Comparative oncogenomics identifies NEDD9 as a melanoma metastasis gene. *Cell* **125**, 1269-1281.

**Kim, S. H., Xia, D., Kim, S. W., Holla, V., Menter, D. G. and Dubois, R. N.** (2010). Human enhancer of filamentation 1 Is a mediator of hypoxia-inducible factor-1alpha-mediated migration in colorectal carcinoma cells. *Cancer Res.* **70**, 4054-4063.

**Kiyokawa, E., Hashimoto, Y., Kurata, T., Sugimura, H. and Matsuda, M.** (1998a). Evidence that DOCK180 up-regulates signals from the CrkII-p130(Cas) complex. *J. Biol. Chem.* **273**, 24479-24484.

**Kiyokawa, E., Hashimoto, Y., Kobayashi, S., Sugimura, H., Kurata, T. and Matsuda, M.** (1998b). Activation of Rac1 by a Crk SH3-binding protein, DOCK180. *Genes. Dev.* **12**, 3331-3336.

**Law, S. F., Estojak, J., Wang, B., Mysliwiec, T., Kruh, G. and Golemis, E. A.** (1996). Human enhancer of filamentation 1, a novel p130cas-like docking protein, associates with focal adhesion kinase and induces pseudohyphal growth in Saccharomyces cerevisiae. *Mol. Cell. Biol.* **16**, 3327-3337.

**Law, S. F., O'Neill, G. M., Fashena, S. J., Einarson, M. B. and Golemis, E. A.** (2000). The docking protein HEF1 is an apoptotic mediator at focal adhesion sites. *Mol. Cell. Biol.* **20**, 5184-5195.

**Lee, H. H., Tien, S. C., Jou, T. S., Chang, Y. C., Jhong, J. G. and Chang, Z. F.** (2010). Src-dependent phosphorylation of ROCK participates in regulation of focal adhesion dynamics. *J. Cell Sci.* **123**, 3368-3377.

**Lee, J. H., Pyon, J. K., Kim, D. W., Lee, S. H., Nam, H. S., Kim, C. H., Kang, S. G., Lee, Y. J., Park, M. Y., Jeong, D. J. et al.** (2010). Elevated c-Src and c-Yes expression in malignant skin cancers. *J. Exp. Clin. Cancer Res.* **29**, 116.

**Li, J., Rix, U., Fang, B., Bai, Y., Edwards, A., Colinge, J., Bennett, K. L., Gao, J., Song, L., Eschrich, S. et al.** (2010). A chemical and phosphoproteomic characterization of dasatinib action in lung cancer. *Nat. Chem. Biol.* **6**, 291-299.

**Li, Y., Bavarva, J. H., Wang, Z., Guo, J., Qian, C., Thibodeau, S. N., Golemis, E. A. and Liu, W.** (2011). HEF1, a novel target of Wnt signaling, promotes colonic cell migration and cancer progression. *Oncogene* **30**, 2633-2643.

**Manie, S. N., Beck, A. R., Astier, A., Law, S. F., Canty, T., Hirai, H., Druker, B. J., Avraham, H., Haghayeghi, N., Sattler, M. et al.** (1997). Involvement of p130(Cas) and p105(HEF1), a novel Cas-like docking protein, in a cytoskeleton-dependent signaling pathway initiated by ligation of integrin or antigen receptor on human B cells. *J. Biol. Chem.* **272**, 4230-4236.

**McLean, G. W., Carragher, N. O., Avizienyte, E., Evans, J., Brunton, V. G. and Frame, M. C.** (2005). The role of focal-adhesion kinase in cancer - a new therapeutic opportunity. *Nat. Rev. Cancer* **5**, 505-515.

**Minegishi, M., Tachibana, K., Sato, T., Iwata, S., Nojima, Y. and Morimoto, C.** (1996). Structure and function of Cas-L, a 105-kD Crk-associated substrate-related protein that is involved in beta 1 integrin-mediated signaling in lymphocytes. *J. Exp. Med.* **184**, 1365-1375.

**Minn, A. J., Gupta, G. P., Siegel, P. M., Bos, P. D., Shu, W., Giri, D. D., Viale, A., Olshen, A. B., Gerald, W. L. and Massague, J.** (2005). Genes that mediate breast cancer metastasis to lung. *Nature* **436**, 518-524.

**Natarajan, M.** (2006). HEF1 is a necessary and specific downstream effector of FAK that promotes the migration of glioblastoma cells. *Oncogene* **25**, 1721-1732.

**Natarajan, M., Stewart, J. E., Golemis, E. A., Pugacheva, E. N., Alexandropoulos, K., Cox, B. D., Wang, W., Grammer, J. R. and Gladson, C. L.** (2006). HEF1 is a necessary and specific downstream effector of FAK that promotes the migration of glioblastoma cells. *Oncogene* **25**, 1721-1732.

**Nojima, Y., Morino, N., Mimura, T., Hamasaki, K., Furuya, H., Sakai, R., Sato, T., Tachibana, K., Morimoto, C., Yazaki, Y. et al.** (1995). Integrin-mediated cell adhesion promotes tyrosine phosphorylation of p130Cas, a Src homology 3-containing molecule having multiple Src homology 2-binding motifs. *J. Biol. Chem.* **270**, 15398-15402.

**Oxley, C. L., Anthis, N. J., Lowe, E. D., Vakonakis, I., Campbell, I. D. and Wegener, K. L.** (2008). An integrin phosphorylation switch: the effect of beta3 integrin tail phosphorylation on Dok1 and talin binding. *J. Biol. Chem.* **283**, 5420-5426.

**Petruzzelli, L., Takami, M. and Herrera, R.** (1996). Adhesion through the interaction of lymphocyte function-associated antigen-1 with intracellular adhesion molecule-1 induces tyrosine phosphorylation of p130cas and its association with c-CrkII. *J. Biol. Chem.* **271**, 7796-7801.

**Pugacheva, E. N. and Golemis, E. A.** (2005). The focal adhesion scaffolding protein HEF1 regulates activation of the Aurora-A and Nek2 kinases at the centrosome. *Nat. Cell Biol.* **7**, 937-946.

**Rosai, J. and Ackerman, L. V.** (2004). *Rosai and Ackerman's Surgical Pathology*. Edinburgh, New York: Mosby.

**Sahai, E. and Marshall, C. J.** (2002). RHO-GTPases and cancer. *Nat. Rev. Cancer* **2**, 133-142.

**Sahai, E. and Marshall, C. J.** (2003). Differing modes of tumour cell invasion have distinct requirements for Rho/ROCK signalling and extracellular proteolysis. *Nat. Cell Biol.* **5**, 711-719.

**Sakai, R., Iwamatsu, A., Hirano, N., Ogawa, S., Tanaka, T., Mano, H., Yazaki, Y. and Hirai, H.** (1994). A novel signaling molecule, p130, forms stable complexes in vivo with v-Crk and v-Src in a tyrosine phosphorylation-dependent manner. *EMBO J.* **13**, 3748-3756.

**Salgia, R.** (1996). p130CAS forms a signaling complex with the adapter protein CRKL in hematopoietic cells transformed by the BCR/ABL oncogene. *J. Biol. Chem.* **271**, 25198-25203.

**Sander, E. E., ten Klooster, J. P., van Delft, S., van der Kammen, R. A. and Collard, J. G.** (1999). Rac downregulates Rho activity: reciprocal balance between both GTPases determines cellular morphology and migratory behavior. *J. Cell Biol.* **147**, 1009-1022.

**Sanz-Moreno, V., Gadea, G., Ahn, J., Paterson, H., Marra, P., Pinner, S., Sahai, E. and Marshall, C. J.** (2008). Rac activation and inactivation control plasticity of tumor cell movement. *Cell* **135**, 510-523.

**Smith, H. W., Marra, P. and Marshall, C. J.** (2008). uPAR promotes formation of the p130Cas-Crk complex to activate Rac through DOCK180. *J. Cell Biol.* **182**, 777-790.

**Viros, A., Fridlyand, J., Bauer, J., Lasithiotakis, K., Garbe, C., Pinkel, D. and Bastian, B. C.** (2008). Improving melanoma classification by integrating genetic and morphologic features. *PLoS Med.* **5**, e120.

**Wolf, K., Mazo, I., Leung, H., Engelke, K., von Andrian, U. H., Deryugina, E. I., Strongin, A. Y., Bröcker, E. B. and Friedl, P.** (2003). Compensation mechanism in tumor cell migration: mesenchymal-amoeboid transition after blocking of pericellular proteolysis. *J. Cell Biol.* **160**, 267-277.

**Xi, X., Flevaris, P., Stojanovic, A., Chishti, A., Phillips, D. R., Lam, S. C. and Du, X.** (2006). Tyrosine phosphorylation of the integrin beta 3 subunit regulates beta 3 cleavage by calpain. *J. Biol. Chem.* **281**, 29426-29430.